# A Study of Boundary-Layer Pressure Adjustments

BARTLETT SMITH AND L. MAHRT

*Atmospheric Sciences Department, Oregon State University, Corvallis 97331*

(Manuscript received 17 October 1979, in final form 20 October 1980)

ABSTRACT

An analytical two-layer approximation of atmospheric flow is developed to study boundary-layer production of vertical motion. The model consists of a boundary layer topped by a free-flow layer. Both layers are time-dependent and possess different values of stratification. The boundary-layer equations are layer-integrated over a fixed depth and surface stress is parameterized using a linearized surface drag law. The dynamics of this modeled flow are quite different from the case of constant eddy viscosity where the boundary layer depth is unrealistically sensitive to the dynamics.

Production of vertical motion is found to be most efficient in the region of the critical latitude where the forcing frequency is comparable to the natural internal frequency of the flow. This internal frequency depends not only on the Coriolis parameter, but also on stratification and boundary-layer properties. For a fixed value of these parameters, the boundary layer produces vertical motion most efficiently when forced at a preferred horizontal length scale.

With sufficiently stratified mesoscale flows, significant boundary-layer pressure adjustments develop which decrease the circulation strength. Stratification is less effective in flows with large horizontal length scale. Results are interpreted for the case of flow forced by oscillating, differential boundary-layer heating.

## 1. Introduction

In this paper we study the influence of stratification on the production of vertical motion in boundary-layer flow driven by time-dependent forcing. In contrast to most previous studies, the present study includes effects of stratification in the boundary layer and emphasizes midlatitude circulations forced by differential heating.

Of importance is that hydrostatic pressure adjustments, induced by vertical motion in the presence of stratification, can significantly reduce the boundary layer production of vertical motion (Lineykin, 1955; Stommel and Veronis, 1957; Walin, 1969; Buzyna and Veronis, 1971; Mahrt and Park, 1976; Shapiro, 1977). The most fundamental example of such interactions is the spindown problem where boundary layer production of vertical motion generates pressure adjustments which act to damp the total pressure gradient field and associated production of vertical motion (Greenspan and Howard, 1963; Holton, 1965). One atmospheric example of such pressure adjustments is the critical latitude effect where the forcing frequency equals the Coriolis frequency. Vertical motion at the critical latitude is inhibited by pressure adjustments as is evident by comparing the studies of Shapiro (1977) and Holton (1975).

Modeled boundary-layer production of vertical motion and interaction with overlying free flow also can depend fundamentally on the parameterization of the boundary layer. Models which assume constant eddy viscosity, without independently restricting the boundary-layer height, predict infinite vertical motion at the critical latitude where the forcing frequency equals the Coriolis frequency (Holton *et al.*, 1971; Yamasaki, 1971). Specification of a finite boundary-layer depth in conjunction with constant eddy viscosity eliminates the vertical motion singularity (Hayashi, 1971; Chang, 1973) at the critical latitude even without pressure adjustments. More realistic solutions seem possible by layer integrating the boundary-layer equations and parameterizing surface stress by means of a surface drag law (e.g., Holton, 1975).

We will use the layer integrated approach to study flows forced by differential, time-dependent boundary-layer heating. Here the boundary-layer flow drives nonturbulent flow aloft in contrast to the abovementioned critical latitude studies where the free-flow pressure field drives the boundary-layer flow. Forcing the flow through boundary-layer heating allows more straightforward analysis of interactions between vertical motion and the pressure field as well as allows examination of some certain aspects of mesoscale and synoptic-scale problems. For example, diurnally varying differential heating can occur where horizontal variations of surface properties or elevation occur such as with sea and land breeze and urban circulation systems.

0022-4928/81/020334-13$07.25

Cloud development may lead to differential surface heating on synoptic scales although such surface heating is normally only a small part of the synoptic circulation problem. In cases where cloud activity is strongly coupled to the subcloud layer, one could generalize the definition of the boundary layer to include the cloud layer. The impetus for this generalization is that turbulent fluxes between the cloud and subcloud layers may be strong in some situations. Of course, if the cloud layer is quite deep, the lack of vertical resolution in the present two-layer model would become a serious limitation.

In order to neglect strong interactions between heating and boundary-layer depth, we will assume the amplitude of the heating to be small. This assumption will also be required to neglect horizontal advections. In contrast to most of the studies cited above, the present study will emphasize midlatitude flows. Therefore, as in Kuo (1973), we will assume constant Coriolis parameter which simplifies the ensuing development. Previous studies of periodically forced midlatitude flows have been motivated primarily in terms of diurnal variation of surface differential heating associated with flow over sloped terrain (Paegle and Rasch, 1973; Holton, 1967). With diurnal forcing, the idealized critical latitude occurs at 30° latitude. However, the influence of such effects on actual weather patterns is uncertain and may be shifted poleward (Paegle and Rasch, 1973).

Although the present study must be considered idealized, since it neglects diurnal variation of certain boundary-layer parameters, it will shed new light on certain aspects of such diurnally forced, midlatitude flows. In the next section we develop the basic equations and parameterization of the boundary layer.

## 2. Layer integrated equations

We partition each field variable as

$$\phi(x,y,z,t) = \phi'(x,y,z,t) + \bar{\phi}(x,y,z,t) + \phi_s(z).$$

The subscript $s$ refers to the height-dependent basic-state value for the undisturbed flow, the overbar refers to the non-turbulent (time-averaged) part of the disturbed flow, and the prime refers to the turbulent deviation from this time average. Assuming local invariance in the $y$ direction, we partition dependence of $\bar{\phi}$ on independent variables as follows:

$$\left.\begin{aligned}
[\bar{u},\bar{v}] &= [u(z,t),v(z,t)]\ \sin x/L \\
[\bar{w},\bar{p},\bar{\theta}] &= [w(z,t),p(z,t),\theta(z,t)]\ \cos x/L \\
[\overline{u'w'},\overline{v'w'}] &= [\overline{\overline{u'w'}}(z,t),\overline{\overline{v'w'}}(z,t)]\ \sin x/L \\
\overline{\theta'w'} &= \overline{\overline{\theta'w'}}(z,t)\ \cos x/L \\
\bar{Q} &= Q^*(z,t)\ \cos x/L
\end{aligned}\right\}, \quad (1)$$

where $u$, $v$ and $w$ are the wind components in the usual $x$, $y$, $z$ Cartesian coordinates, $p$ the pressure, $\theta$ the potential temperature, $\rho$ the density, $f$ the Coriolis parameter, $g$ the acceleration of gravity, $L$ the horizontal length scale of the imposed forcing, and $Q^*$ the amplitude of clear air diabatic heating. The above partitioning filters out propagating waves by requiring any forced or unforced oscillation to be spatially fixed, allowing only standing wave type of solutions. Substituting these expressions into the governing equations for small-amplitude (small Rossby number), hydrostatic, Boussinesq flow produces the following system of equations for the height and time-dependent complex amplitudes:

$$\frac{\partial u}{\partial t} - fv = \frac{p}{\rho_s L} - \frac{\partial}{\partial z}\overline{\overline{u'w'}} \quad (2)$$

$$\frac{\partial v}{\partial t} + fu = -\frac{\partial}{\partial z}\overline{\overline{v'w'}} \quad (3)$$

$$\frac{\partial p}{\partial z} = \rho_s g \frac{\theta}{\theta_s} \quad (4)$$

$$\frac{\partial \theta}{\partial t} + w\theta_s \frac{N^2}{g} = -\frac{\partial}{\partial z}\overline{\overline{\theta'w'}} + Q^* \quad (5)$$

$$\frac{u}{L} + \frac{\partial w}{\partial z} = 0 \quad (6)$$

$$N^2 \equiv \frac{g}{\theta_s}\frac{d\theta_s}{dz} = \text{Brunt-Väisälä frequency.}$$

We integrate the equations from the surface layer, $z = 0$, to a specified constant height $h$, where turbulent fluxes are assumed to be always negligible. This layer is assumed to be characterized by constant stratification corresponding to Brunt-Väisälä frequency $N_B$. Turbulent fluxes are neglected in an overlying layer of free flow, extending from $z = h$ to the top of the atmosphere and characterized by Brunt-Väisälä frequency $N_f$.

The specification of constant boundary-layer depth requires additional comment. The boundary-layer turbulence and depth are often considered to scale with some function of $u_*/f$, where $u_*$ is the surface friction velocity and $f$ is the Coriolis parameter. Since the role of the Coriolis effects on the turbulent covariance budgets is normally considered to be unimportant, the Coriolis parameter influences the turbulence and stress field mainly through the influence of the momentum equation on the mean shear, as implied in the Ekman dynamics for stationary flow. However, with accelerations the role of the Coriolis parameter on the boundary-layer depth may be quite different, as occurs with the hypothetical critical latitude effect and as may occur with nocturnal inertial oscillations. Models of turbulence and boundary-layer depth normally neglect this interaction between accelerations and mean shear as

well as neglect the influence of mean vertical motion on boundary layer depth. On the other hand, most dynamical studies usually neglect the role of other constraints on the boundary-layer depth such as stratification and dissipation of turbulence. Simultaneous inclusion of all of these influences is a complicated and unresolved problem. Thus, within the context of this study the assumption of constant boundary-layer depth seems as justifiable as any alternate simple parameterization.

There are some atmospheric situations where the boundary-layer depth is approximately constant in association with large-scale or cloud-induced subsidence although fluxes at the boundary-layer top may still be significant in these cases due to entrainment. One could specify $h$ to be just above maximum boundary-layer depth which would allow layer integration of the equations with neglect of fluxes at $h$. In the present study we will specify constant boundary-layer depth but consider this case as an informative asymptotic case rather than representative of special atmospheric conditions.

Vertical integration of the boundary-layer equations (2)–(6) over the constant depth $h$ produces a system of equations for the boundary-layer-averaged fields, where

$$(\overline{\ })^h \equiv h^{-1}\int_0^h (\ )dz. \tag{7}$$

Since the scale height for the basic-state fields $\theta_s$ and $\rho_s$ is typically much larger than the boundary-layer height, we can replace the height-dependent undisturbed fields, to a good approximation, with their layer-averaged values $\theta_0$ and $\rho_0$. Layer-integrating (2)–(6), we obtain

$$\frac{d\bar{u}^h}{dt} - f\bar{v}^h = \frac{\bar{p}^h}{\rho_0 L} + \frac{\overline{\overline{(u'w')}}_0}{h}, \tag{8}$$

$$\frac{d\bar{v}^h}{dt} + f\bar{u}^h = \frac{\overline{\overline{(v'w')}}_0}{h}, \tag{9}$$

$$\frac{p(h,t) - p(0,t)}{h} = \rho_0 g \frac{\bar{\theta}^h}{\theta_0}, \tag{10}$$

$$\frac{d\bar{\theta}^h}{dt} + \bar{w}^h \frac{\theta_0}{g} N_B{}^2 = \frac{\overline{\overline{(\theta'w')}}_0}{h} + h^{-1}\int_0^h Q^* dz, \tag{11}$$

$$\frac{\bar{u}^h}{L} + \frac{w(h,t)}{h} = 0. \tag{12}$$

Vertical motion in the surface layer is assumed to be negligible compared to $w(h)$.

Surface stress will be parameterized using a linearized drag law,

$$\overline{\overline{(u'w')}}_0 = -C_D V(\bar{u}^h \cos\eta - \bar{v}^h \sin\eta), \tag{13}$$

$$\overline{\overline{(v'w')}}_0 = -C_D V(\bar{v}^h \cos\eta + \bar{u}^h \sin\eta), \tag{14}$$

where $C_D$ is a specified constant drag coefficient, $V$ is a scale velocity, and $\eta$ is the specified constant angle between the surface stress and the layer mean wind. Relating the stress to the layer-averaged winds instead of surface winds has several practical advantages when estimating drag coefficients from actual data. Layer-averaged winds are less sensitive to local inhomogeneity and less dependent on the drag coefficient itself. Furthermore, use of surface winds require selection of an arbitrary height near the surface where, unfortunately, the wind varies most rapidly with height. On the other hand, use of layer-averaged winds requires specification of the boundary-layer top as well as knowledge of wind profiles.

We estimated values of the drag coefficient (Fig. 1) defined by Eqs. (13)–(14) from Wangara data (Clarke *et al.*, 1971) by choosing the boundary-layer top to be the inversion heights computed by Melgarejo and Deardorff (1974) for daytime mixed-layer cases. For stable boundary-layer cases, we choose the boundary-layer top to be the height of the nocturnal low-level jet or the top of the layer of significant shear. These values of $h$ are close, but not always identical to the top of the momentum boundary layer $h_u$ estimated by Melgarejo and Deardorff (1974). Observations with layer-averaged speeds $< 2$ m s$^{-1}$ (two cases) are discarded. To compute $C_D$, we then assign the velocity scale $V$ to be the actual layer-averaged wind. Values of the drag coefficient so computed are very sensitive to stability at near-neutral values of stability but then somewhat independent of stability with significant stratification (Fig. 1). The latter property is quite advantageous since linear models of the boundary layer require constant drag coefficient.

The angle $\eta$ is probably quite sensitive to baroclinity and thus differential heating as is the case for the surface cross isobar flow angle (e.g., Arya and Wyngaard, 1975). In the present linear model, we specify $\eta$ independently of the flow. The ensuing dynamics will be found to be rather insensitive to the value of $\eta$. Since $C_D$ and $h$ are assumed constant in time, we are also neglecting important interactions of the boundary layer with surface heat fluxes and vertical motions. However, it will be shown that the ratio $C_D/h$ is the controlling frictional factor which, in actual atmospheric flows, usually varies much less than either $C_D$ or $h$. The velocity scale $V$ can be related to the specified forcing such as surface heating or pressure gradient at the top of the model as will be done in Section 5.

In order to close the layer-averaged system of Eqs. (8)–(14), we introduce two boundary-layer structure parameters $r$ and $s$ which relate layer-averaged pressure and vertical motion to values at the boundary-layer top and bottom. These structure parameters are defined so that

$$\bar{p}^h = \frac{rp(h,t) + p(0,t)}{r+1}, \tag{15}$$

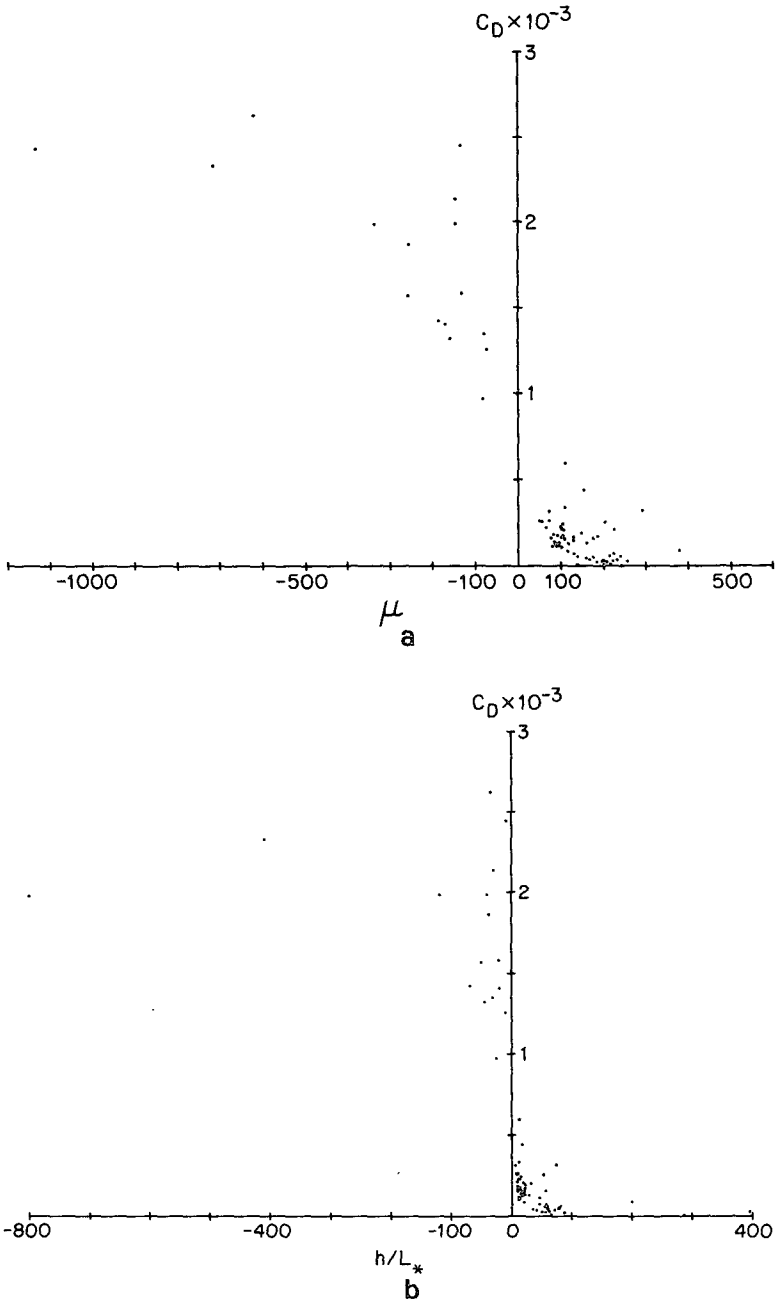


FIG. 1. The drag coefficient as a function of the stability parameter $\mu = u_*/fL_*$ (a) and $h/L_*$ (b), where $u_*$, the surface friction velocity, and $L_*$, the Monin-Obukhov length, are from Melgarejo and Deardorff (1974).

$$\bar{w}^h = \frac{s}{s+1} w(h,t). \quad (16)$$

If pressure adjustments in the boundary layer are neglected, the introduction of $s$ is not required.

These layer-averaged values correspond to general profiles of the form

$$p(z,t) = p(h,t) + (1 - z/h)^r[p(0,t) - p(h,t)], \quad (17)$$

$$w(z,t) = w(h,t)[1 - (1 - z/h)^s]. \quad (18)$$

For example, a well-mixed layer would assume values of $(r,s) = 1$, while exponential profiles for $\theta$ and $u$ with $e^{-1}$ folding height $h$, as in Ekman flow, correspond to $(r,s) = 1.4$. The structure parameters are not very sensitive to different theoretical profiles nor will the dynamics of different flow situations turn out to be very sensitive to the structure parameters. In fact, the discussion of physical interactions presented here does not require determination of

these structure functions. They are merely specified for mathematical completeness.

Combining (8)–(14) and (15)–(16) results in a single equation for pressure and vertical motion at the boundary-layer top:

$$\left[\left(f + \frac{C_D V}{h}\sin\eta\right)^2 + \left(\frac{d}{dt} + \frac{C_D V}{h}\cos\eta\right)^2\right]\frac{d}{dt}w(h,t)$$
$$+ \frac{s}{(s+1)(r+1)}\frac{h^2}{L^2}N_B{}^2\left(\frac{d}{dt} + \frac{C_D V}{h}\cos\eta\right)w(h,t)$$
$$+ \frac{h}{\rho_{0L}{}^2}\left(\frac{d}{dt} + \frac{C_D V}{h}\cos\eta\right)\frac{d}{dt}p(h,t)$$
$$= \frac{h}{L}\frac{g}{(r+1)\theta_0}\left(\frac{d}{dt} + \frac{C_D V}{h}\cos\eta\right)\frac{Q}{L}, \quad (19)$$

where

$$Q \equiv \overline{(\theta' w')}_0 + \int_0^h Q^* dz.$$

Eq. (19) describes boundary-layer production of vertical motion as a function of forcing due to differential boundary-layer heating and the pressure field induced on the boundary layer by the frictionless flow aloft. The second term represents enhanced boundary-layer pressure adjustments due to interaction of the vertical motion field and boundary-layer stratification.

In the steady-state limit, Eq. (19) reduces to the layer-averaged thermodynamic equation for steady boundary-layer flow in which case the vertical motion amplitude is

$$\frac{s}{(s+1)}w(h) = \bar{w}^h = \frac{g}{\theta_0}\frac{Q}{N_B h}.$$

As in Stommel and Veronis (1957), vertical motion is linearly proportional to the inverse of stratification.

## 3. The two-layer system

In order to retain dynamical coupling between the frictionless flow and the time-dependent boundary layer, we will calculate pressure adjustments in the flow aloft due to boundary-layer production of vertical motion. These pressure adjustments aloft are, in turn, hydrostatically induced on the boundary layer.

Neglecting turbulent fluxes and diabatic heating in (2)–(6), we obtain the following equations for the frictionless flow above the boundary layer ($z \geq h$), where variables are subscripted with $f$:

$$\frac{\partial u_f}{\partial t} - f v_f = \frac{p_f}{\rho_s L} \quad (20)$$

$$\frac{\partial v_f}{\partial t} + f u_f = 0 \quad (21)$$

$$\frac{\partial p_f}{\partial z} = \rho_s g \frac{\theta_f}{\theta_s} \quad (22)$$

$$\frac{\partial \theta}{\partial t} + w_f \frac{\theta_s}{g} N_f^2 = 0 \quad (23)$$

$$\frac{u_f}{L} + \frac{\partial w_f}{\partial z} = 0. \quad (24)$$

In this layer, vertical motion in the presence of stratification drives temperature adjustments which in turn correspond to hydrostatic pressure adjustments. Combining (20), (21) and (24) produces an equation which relates pressure adjustments to vertical motion in the frictionless layer

$$\frac{1}{\rho_s L^2}\frac{\partial}{\partial t}p_f(z,t) = -\left(\frac{\partial^2}{\partial t^2} + f^2\right)\frac{\partial}{\partial t}w_f(z,t). \quad (25)$$

If pressure adjustments in the free flow are confined to a depth much shallower than the scale height for $\theta_s$ and $\rho_s$, the basic state can be approximated with constant values $\theta_0$ and $\rho_0$. By evaluating the depth scale in (28) we can see that this restriction will be valid in mesoscale and smaller scale flows or flows with strong stratification. Combining Eqs. (22), (23), and (25) leads to a single equation for pressure or vertical motion:

$$\left[\left(\frac{\partial^2}{\partial t^2} + f^2\right)\frac{\partial^2}{\partial z^2} - \frac{N_f^2}{L^2}\right][p_f(z,t), w_f(z,t)] = 0. \quad (26)$$

The two-layer system is closed by invoking continuity of pressure and vertical motion at the interface $h$ and specifying pressure at the top of the free flow. Here we assume vanishing pressure at the free-flow top.

Since we are interested in the coupling mechanisms between the time-dependent boundary layer and the frictionless flow, we will consider only the case in which the boundary layer and overlying flow oscillate and decay with the same frequency and time constant. Pressure adjustments in the frictionless flow are then due to boundary layer production of vertical motion alone, and exclude adjustments due to oscillating free modes not associated with boundary-layer convergence.

The flow response forced by the boundary conditions, such as surface heating, is obtained by solving (19), (25) and (26). However, before examining the amplitude and phase of the forced response in Section 5, we first study unforced modes for this two-layer system.

## 4. Unforced modes

To examine the unforced modes of the boundary layer-free flow system, we assume a general time-dependence of the form

$$[p_f(z,t),w_f(z,t)] = [p_f(z),w_f(z)]e^{\alpha t}. \quad (27)$$

Normally, the frequency $\alpha$ is complex leading to both oscillating and damped responses. From (26), the height-dependent amplitudes in the free flow ($z \geq h$) are

$$[p_f(z),w_f(z)] = [p(h),w(h)] \exp\left[\frac{-N_f}{L}\frac{(z-h)}{(f^2+\alpha^2)^{1/2}}\right]. \quad (28)$$

Here $L(f^2+\alpha^2)^{1/2}/N_f$ is the depth scale of the oscillating Lineykin layer (Park and Mahrt, 1979) where pressure adjustments occur in response to boundary-layer production of vertical motion.

Substituting the expressions for $p_f$ and $w_f$ into (25) and combining this with the unforced version of the boundary-layer equation (19), we obtain a sixth-order polynomial in $\alpha$,

$$\left[\left(f+\frac{C_DV}{h}\sin\eta\right)^2+\left(\alpha+\frac{C_DV}{h}\cos\eta\right)^2\right]\alpha + \frac{s}{(s+1)(r+1)}\frac{h^2}{L^2}N_B{}^2\left(\alpha+\frac{C_DV}{h}\cos\eta\right) + \frac{h}{L}N_f(f^2+\alpha^2)^{1/2}\left(\alpha+\frac{C_DV}{h}\cos\eta\right)=0. \quad (29)$$

The six roots of this characteristic equation represent the possible free oscillating and dampening modes in the two-layer system. Dividing by $f^3$ transforms (29) into nondimensional form

$$[(1+\hat{C}_D\sin\eta)^2+(\hat{\alpha}+\hat{C}_D\cos\eta)^2]\hat{\alpha} + A^2\hat{B}^2(\hat{\alpha}+\hat{C}_D\cos\eta) + \hat{B}(1+\hat{\alpha}^2)^{1/2}(\hat{\alpha}+\hat{C}_D\cos\eta)=0, \quad (30)$$

where

$\hat{\alpha}$ dimensionless complex frequency $[\equiv\alpha/f]$

$\hat{B}$ free-flow stratification parameter $[\equiv hN_f/Lf]$

$\hat{C}_D$ scaled drag coefficient $[\equiv C_DV/hf]$

$A$ boundary-layer stratification parameter $\left\{\equiv\left[\frac{s}{(s+1)(r+1)}\right]^{1/2}\frac{N_B}{N_f}\right\}$.

The relative size of the nondimensional parameters $\hat{B}$, $\hat{C}_D$ and $A$ determines the nature of the unforced modes subject to the initial conditions imposed on the flow. The scaled drag coefficient $\hat{C}_D$ can be interpreted as the ratio of the inertial time scale to the time scale for turbulent diffusion through the boundary layer. The importance of pressure adjustments in the free flow is proportional to the stratification parameter $\hat{B}$. The value of $A$ is an indication of the relative importance of pressure adjustments in the boundary layer compared to pressure adjustments aloft. For a well-mixed boundary layer, $A = 0$, but in a nocturnal boundary layer with strong radiative cooling near the surface, $A$ is normally $>1$.

The roots to (30) can be calculated numerically through successive approximations for given values of the flow parameters. An alternative approach is to expand $\hat{\alpha}$ in some small parameter and investigate the asymptotic solution to (30) in terms of the variables $\hat{B}$, $\hat{C}_D$ and $A$. For example, if the two layers are weakly stratified or if the aspect ratio is small, we could expand $\hat{\alpha}$ in the small parameter $\hat{B}$, i.e.,

$$\hat{\alpha} = \alpha_0 + \hat{B}\alpha_1 + \hat{B}^2\alpha_2 + \ldots. \quad (31)$$

Substituting this expression into the polynomial equation (30) and taking the limit $\hat{B} \to 0$, Eq. (30) yields a cubic relationship in $\alpha_0$

$$[(1+\hat{C}_D\sin\eta)^2+(\alpha_0+\hat{C}_D\cos\eta)^2]\alpha_0 = 0, \quad (32)$$

with the following roots:

$$\alpha_0 = 0 \quad (33a)$$

$$\alpha_0 = -\hat{C}_D\cos\eta - i(1+\hat{C}_D\sin\eta) \quad (33b)$$

$$\alpha_0 = -\hat{C}_D\cos\eta + i(1+\hat{C}_D\sin\eta). \quad (33c)$$

The root $\alpha_0 = 0$ represents the zero-order stationary state in which the pressure gradient force, Coriolis and frictional forces are in balance. Heating due to turbulent heat flux is balanced by adiabatic cooling. The second root (33b) represents an inertial oscillation.

Corrections to the balanced flow (33a) resulting from $O(\hat{B})$ and $O(\hat{B})^2$ pressure adjustments are

$$\alpha_1 = \frac{-\hat{C}_D\cos\eta}{(1+\hat{C}_D\sin\eta)^2+(\hat{C}_D\cos\eta)^2}, \quad (34)$$

$$\alpha_2 = \frac{-\hat{C}_D\cos\eta(2\alpha_1{}^2+A^2)-\alpha_1}{(1+\hat{C}_D\sin\eta)^2+(\hat{C}_D\cos\eta)^2}. \quad (35)$$

The first-order correction (34) represents pressure adjustments generated in the free flow and imposed upon the boundary layer. The time scale associated with the spindown of an initial disturbance ($e^{-1}$ folding time) to this order is similar to that obtained in Mahrt and Park (1976) and here assumes the form

$$t_d \approx -(\hat{B}\alpha_1 f)^{-1} = \frac{L}{hN_f}\left[\frac{(1+\hat{C}_D\sin\eta)^2+(\hat{C}_D\cos\eta)^2}{\hat{C}_D\cos\eta}\right]. \quad (36)$$

Within this time, an initial disturbance will lose most of its kinetic energy through conversion to available potential energy associated with adiabatic cooling in the free layer.

The order $\hat{B}^2$ correction, (35), includes the effect of pressure adjustments within the boundary layer, as well as corrections to pressure adjustments aloft. This correction makes the estimate for $\hat{\alpha}$ more nega-

tive, which shortens the spindown time. Here the lifetime of an initial disturbance decreases due to pressure adjustments in the boundary layer as well as aloft.

Higher order corrections do not introduce any new physical mechanisms, and are negligibly small compared to the second-order result with weak stratification ($\hat{B} \ll 1$).

The first-order correction to the damped inertial oscillation (33b) is

$$\alpha_1 = -\frac{(1+\alpha_0^2)^{1/2}}{2\alpha_0}. \tag{37}$$

For any value of $\hat{C}_D$, the real part of $\alpha_1$ is positive so that the lifetime of the damped inertial oscillation is extended in the presence of the order $\hat{B}$ pressure adjustments in contrast to spindown.

## 5. Differential heating

We now consider vertical motion forced by differential heating with vanishing pressure gradient at the top of the free layer. This heating is of the form

$$Q = Q_0 e^{-i\omega t} \tag{38a}$$

in which case the vertical motion response is

$$w(h,t) = W(h)e^{-i\omega t}, \tag{38b}$$

where $W(h)$ is the unknown complex amplitude and $\omega$ is the specified forcing frequency. Using the thermal wind relationship for the geostrophic wind $v_g$, we estimate the horizontal velocity scale to be

$$V \approx |v_g(0) - v_g(h)| = \frac{h}{L}\frac{g}{f}\left|\frac{\bar{\theta}^h}{\theta_0}\right| \approx \frac{g}{\omega f \theta_0}\frac{|Q_0|}{L}. \tag{38c}$$

Substituting (38b) into (19), and using the frictionless flow equations (25) and (26), leads to the following expression for the forced response:

$$W(h) = \frac{gQ_0(1-G)^{-1}}{(r+1)N_f L\theta_0(f^2-\omega^2)^{1/2}}, \tag{39}$$

where

$$G = \frac{i\omega L}{hN_f(f^2-\omega^2)^{1/2}}\left[\frac{C_D V}{h}\cos\eta - i\omega + \left(f + \frac{C_D V}{h}\sin\eta\right)^2\left(\frac{C_D V}{h}\cos\eta - i\omega\right)^{-1} + i\frac{h^2}{L^2}\frac{s}{(s+1)(r+1)}\frac{N_B^2}{\omega}\right].$$

Note that $w(h)$ is finite at $f = \omega$ due to canceling effects in the numerator and denominator. This solution is sufficiently complicated that it is most easily interpreted by holding certain variables constant. In the ensuing discussion we will consider the forcing frequency $\omega$ and the vertical velocity scale $W_s$ to be constant. The latter is given by

$$W_s = \frac{gQ_0}{(r+1)N_f L\theta_0\omega}. \tag{40a}$$

The solution for the scaled vertical motion

$$\hat{w} \equiv W(h)/W_s \tag{40b}$$

from (39) becomes

$$\hat{w} = \left[(f^{*2}-1)^{1/2}\frac{i}{B^*}\left\{(C_D^*\cos\eta - i) \times \left[1 + \left(\frac{f^* + C_D^*\sin\eta}{C_D^*\cos\eta - i}\right)^2\right] + iA^2B^{*2}\right\}\right]^{-1}, \tag{40c}$$

where

$$f^* \equiv f/\omega = \text{scaled latitude},$$

$$B^* \equiv \frac{hN_f}{L\omega} = f^*\hat{B},$$

$$C_D^* \equiv \frac{C_D V}{h\omega} = f^*\hat{C}_D.$$

It is apparent from (40a) that rescaling would be necessary in order to examine the case of a neutrally stratified flow aloft. In this case the flow aloft is nondivergent [$W_f = W(h)$, $P_f = 0$] and does not influence the boundary-layer dynamics. The steady-state limit ($\omega \to 0$) has already been discussed in Section 2.

The vertical velocity scale $W_s$ is proportional to the strength of the differential heating which dictates the generation of available potential energy. The vertical velocity scale also is inversely proportional to the Brunt-Väisälä frequency. Stratification is automatically important in the present study as opposed to classical Ekman dynamics with constant viscosity or constant eddy viscosity. In Ekman dynamics with small stratification parameter, temperature diffusion can drive significant temperature and pressure adjustments even outside the Ekman layer and by comparison, pressure adjustments due to vertical advection of density or potential temperature may be unimportant (Barcilon and Pedlosky, 1967). However, in the present study, turbulent diffusion of temperature is neglected outside the boundary layer so that temperature and pressure adjustments are driven only by vertical advection of potential temperature (adiabatic cooling).

It is noteworthy that the vertical velocity scale varies only as the inverse of the square root of the vertical gradient of potential temperature. Thus, for a given surface differential heating rate, this velocity scale is more sensitive to the horizontal length scale. The vertical velocity scale is also inversely related to the forcing frequency. Smaller forcing frequency means that the differential heating can generate

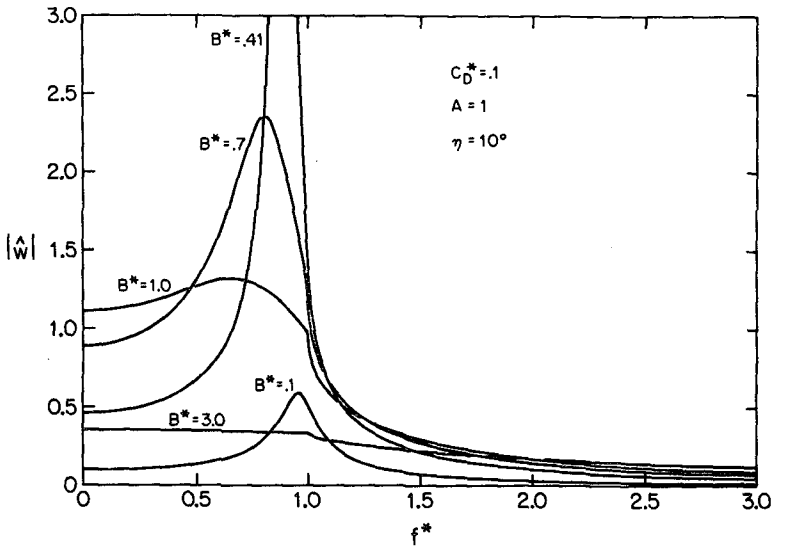


FIG. 2. Scaled vertical velocity (40c) as a function of scaled latitude for several different values of $B^*$. For $B^* = 0.41$, the maximum value of $|\hat{w}|$ is 490.

horizontal pressure gradients over a longer period before reversing sign. The efficiency of generation of boundary-layer vertical motion, for a given vertical velocity scale, depends on latitude, stratification parameter $B^*$ and scaled drag coefficient $C_D^*$, as is evident in (40c).

The scaled drag coefficient can be interpreted as being proportional to the ratio of the forcing time scale ($1/\omega$) to the boundary-layer diffusion time scale ($h/C_DV$). Thus other factors constant, frictional effects more strongly modify the dynamics of synoptic circulations than diurnally forced flows. Since both $C_D$ and $h$ typically decrease by an order of magnitude from day to night and $C_D^*$ is proportional to $C_D/h$, the scaled drag coefficient may not be particularly sensitive to diurnal variations of the actual drag coefficient and boundary-layer depth. Then $C_D^*$ depends mainly on wind speed and forcing frequency for a given surface roughness. In the examples below, we choose $C_D^* = 0.1$ which characterizes both diurnal forcing, and synoptic forcing with weak winds and/or small surface roughness. For example with diurnal forcing, a layer-averaged wind speed of 5 m s$^{-1}$ and Wangara values of the drag coefficient, we construct the following two estimates of $C_D^*$. In the daytime, the drag coefficient (Fig. 1) and boundary-layer depth are typically $\sim 2.5 \times 10^{-3}$ and 1 km, respectively, in which case $C_D^*$ is $\sim 0.17$. At night typical values are $C_D = 3 \times 10^{-4}$ and $h = 200$ m in which case $C_D^*$ is approximately 0.10.

### *a. Critical latitude position*

We first estimate the influence of pressure adjustments and drag coefficient on the position of the critical latitude. We are not interested in the detailed structure of the flow since the present linear theory neglects advections which are particularly important near the actual critical latitude. For diurnal variations, $\omega$ is $\sim 7 \times 10^{-5}$ s$^{-1}$. Then the classical Ekman-critical latitude ($f^* = 1$) corresponds to 30° latitude and 45° latitude corresponds to $f^* = 1.4$. Because we assume that the Coriolis parameter is locally constant, the present study is only indirectly related to the synoptic-scale critical latitude which is thought to occur between 5 and 10° latitude.

Figs. 2 and 3 show the scaled vertical motion as a function of nondimensional latitude for various values of the stratification parameter and scaled drag coefficient for the case where the boundary-layer and free-flow stratification are approximately equal. The maximum vertical motion in both figures is shifted equatorward of the classical Ekman critical latitude, $f^* = 1$. In this model, maximum convergence occurs at the latitude where the natural frequency of the unforced mode matches the forcing frequency. This natural internal frequency, and thus the latitudinal shift, depend on stratification parameters and boundary-layer properties.

For example, internal gravity wave theory indicates that an increase in stratification or aspect ratio increases the internal oscillation frequency (Eckart, 1960). The increase of internal frequency due to increasing stratification parameter is evident in the present flow situation through an equatorward shift of the maximum vertical motion response with increasing stratification parameter (Fig. 2). For $N_f \sim 10^{-2}$ s$^{-1}$, $h \sim 1$ km and $\omega = 7.3 \times 10^{-5}$ s$^{-1}$, the parameter $B^*$ is approximately $(L/100\text{ km})^{-1}$. Thus,

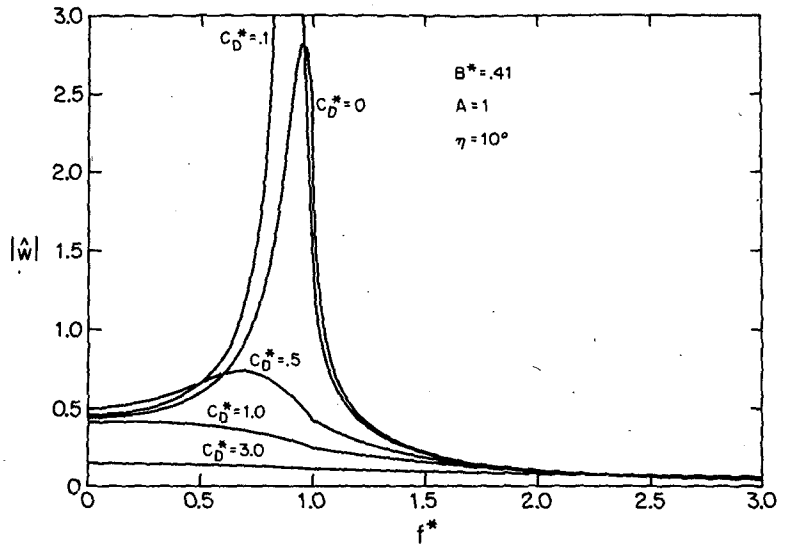


FIG. 3. As in Fig. 2 except for several different values of $C_D^*$. For $C_D^* = 0.1$, the maximum value of $|\hat{w}|$ is 490.

$B^*$ is typically O(0.1) for synoptic-scale flows, O(1) for mesoscale flows and O(10) for very local nocturnal circulations.

The equatorward shift of maximum vertical motion also increases with scaled drag coefficient (Fig. 3), as can be explained through the unforced mode calculations in the previous section. Neglecting pressure adjustments, the natural frequency of the frictionally damped inertial oscillation is (33b)

$$\omega_n = -\left(f + \frac{C_D V}{h} \sin\eta\right). \tag{41}$$

Dividing through by $\omega$ and solving for the critical latitude ($\omega = \omega_n$),

$$f^*_{\text{crit}} = C_D^* \sin\eta, \tag{42}$$

we obtain an equatorward shift which increases linearly with $C_D^*$. Since $C_D^*$ is typically O(0.1) and $\eta$ is normally less than 30° (Fig. 1), the frictionally induced latitudinal shift is usually small.

### b. *Preferred length scale and drag coefficient*

For a fixed vertical velocity scale and forcing frequency, the vertical motion response increases with the value of the stratification parameter $B^*$, until some preferred value, and then decreases with further

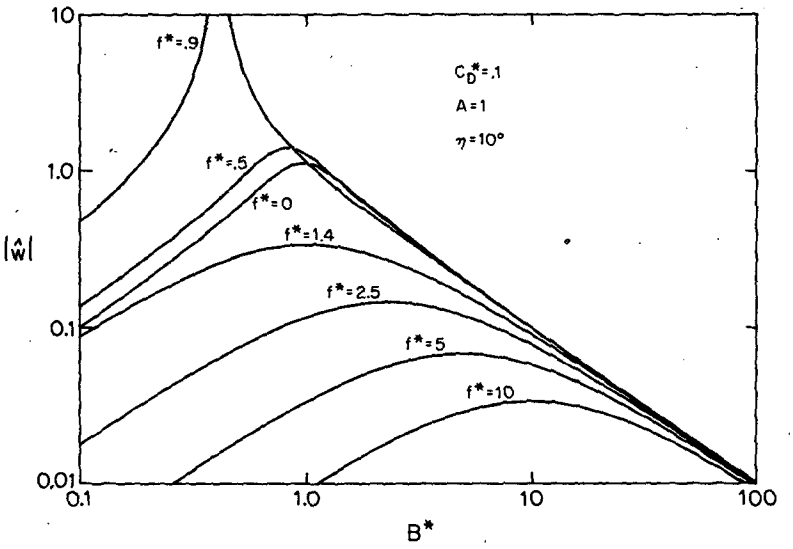


FIG. 4. Scaled vertical velocity (40c) as a function of stratification parameter for several different values of $f^*$. For $f^* = 0.9$, the maximum value of $|\hat{w}|$ is 169.

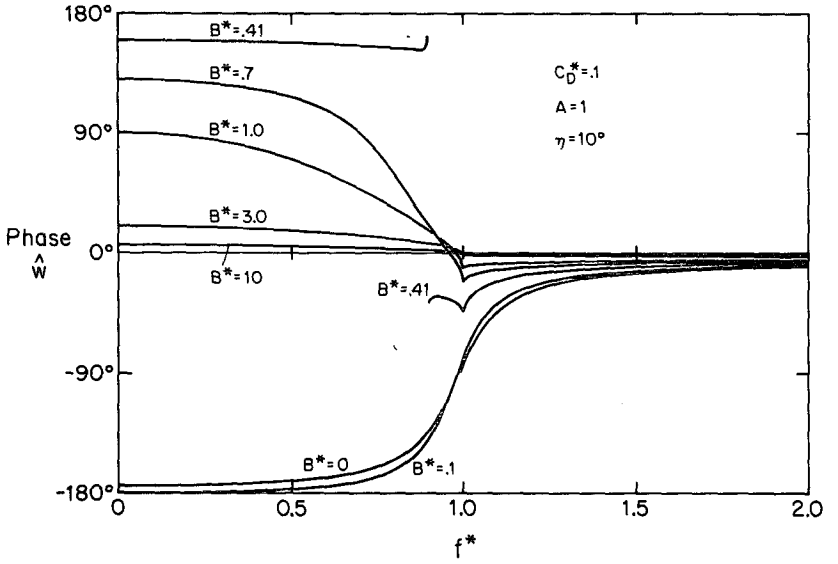


FIG. 5. Phase of vertical velocity (40c) as a function of scaled latitude for several different values of $B^*$.

increase of $B^*$ (Figs. 2 and 4). That is, for a given vertical velocity scale, forcing frequency and scaled drag coefficient, the maximum vertical velocity is generated at a preferred horizontal length scale. At smaller scales, pressure effects more efficiently damp out vertical motions. At larger scales, convergence becomes too spread out to efficiently generate vertical motion. At the critical latitude ($f^* \approx 0.9$) and $C_D^* = 0.1$, the maximum vertical motion occurs at $B^* = 0.41$. For $N_f = 10^{-2}$ s$^{-1}$ and $h = 1$ km, the corresponding length for diurnal oscillations is $L_D \equiv hN_f/0.41\omega \approx 335$ km. The behavior of the scaled vertical motion at a fixed latitude (Fig. 4) exhibits a similar dependence on $B^*$ and the horizontal length scale.

The resonant response also reaches a relative maximum for a preferred value of the scaled drag coefficient $C_D^*$ (Fig. 3). This behavior is due to the two opposing influences of friction on cross-isobar flow (Mahrt, 1974). The surface stress simultaneously rotates the wind towards the pressure gradient force vector and reduces the flow speed. For small $C_D^*$, the surface drag primarily rotates the wind vector with less important reduction of wind speed so that the cross-isobar flow increases with $C_D^*$. For larger values of $C_D^*$, the effect of decreasing flow speed exceeds the effect due to rotation of the wind vector. Then increasing drag coefficient *reduces* the cross-isobar flow and convergence.

The influence of friction and pressure adjustments on low-level convergence is greatest near the critical latitude and decreases poleward (Figs. 2 and 3). Thus, studies based on one fixed latitude (e.g., Shapiro, 1977) cannot be used to assess the general importance of boundary-layer friction and coupling between the boundary layer and free flow.

### c. *Vertical motion phase*

In Figs. 5 and 6, the phase of the response with respect to the forcing is plotted as a function of latitude for different values of $B^*$ and $C_D^*$, respectively. The response lags the forcing by less than a quarter cycle poleward of the critical latitude, but equatorward, the phase lag of the response is quite complicated. As frictional effects become more important than accelerations and pressure adjustments (increasing $C_D^*$), the phase lag poleward of the critical latitude increases (Fig. 6) toward the asymptotic value of 90°.

Pressure adjustments associated with the stratification increase the adjustment rate of the flow and decrease the phase lag of the response poleward of the critical latitude. Walsh (1974) also showed that increased stratification could significantly reduce the phase lag for sea breeze circulations north of the critical latitude ($f^* = 1.5$). As $B^*$ approaches infinity, as would occur with vanishing horizontal length scale and finite stratification, the response becomes in phase with the forcing (Fig. 5) for all latitudes. Then turbulent heat flux is balanced primarily by adiabatic cooling as in the physics of the $E^{1/3}$ layer (Park and Mahrt, 1979, Table 1).

At the critical latitude $f^* = 0.9$, there is a 180° phase shift under the resonant conditions $B^* = 0.41$, $C_D^* = 0.1$ (Figs. 6 and 7). This shift is discussed by Holton *et al.* (1971) for the Ekman case and is analogous to the phase shift for resonant forcing of a damped harmonic oscillator (e.g., Feynman, 1964).

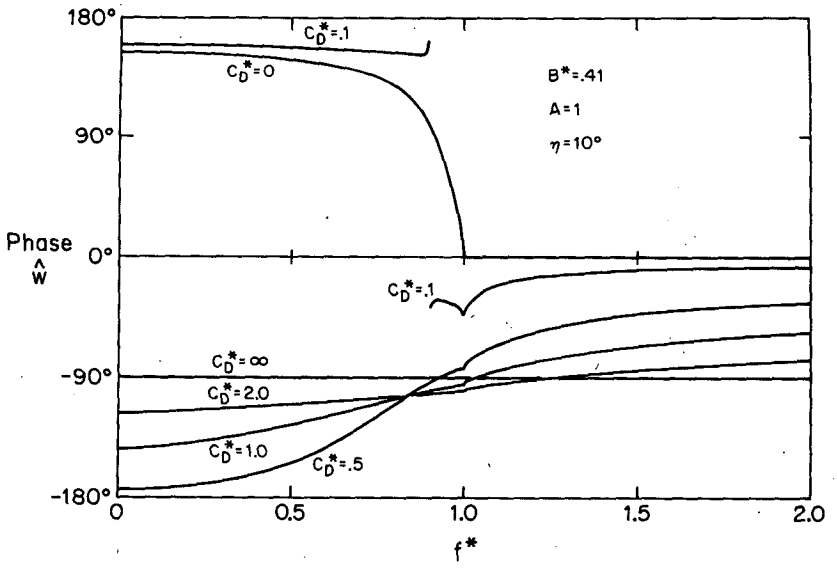


FIG. 6. As in Fig. 5 except for several different values of $C_D^*$.

*d. Modified boundary-layer stratification*

When the boundary-layer stratification is enhanced beyond that of the background free flow stratification (Fig. 7), the production of vertical motion is reduced due to increased pressure adjustments in the boundary layer. Since stratification is particularly effective at small scales, the preferred length scale of maximum vertical motion production increases with increased boundary-layer stratification.

The influence of boundary-layer stratification may be particularly important in the case of a stable boundary-layer driven by surface radiational cooling with weak stratification aloft. The Brunt-Väisälä frequency of the nocturnal boundary layer is typically $2-3 \times 10^{-2}$ s$^{-1}$ but can be as high as $5 \times 10^{-2}$ s$^{-1}$ (see the case study of Merrill, 1977) and even higher in some high-latitude winter time boundary layers over a snow surface. We note that the free atmosphere Brunt-Väisälä frequency is typically $\sim 10^{-2}$ s$^{-1}$, and note that the factor in $A$ describing profiles of velocity and potential temperature [see Eq. (30)] is less than one in the stable boundary layer (½ for linear profiles). Then values of $A$ for the stable boundary layer will typically range from about 1–about 3.

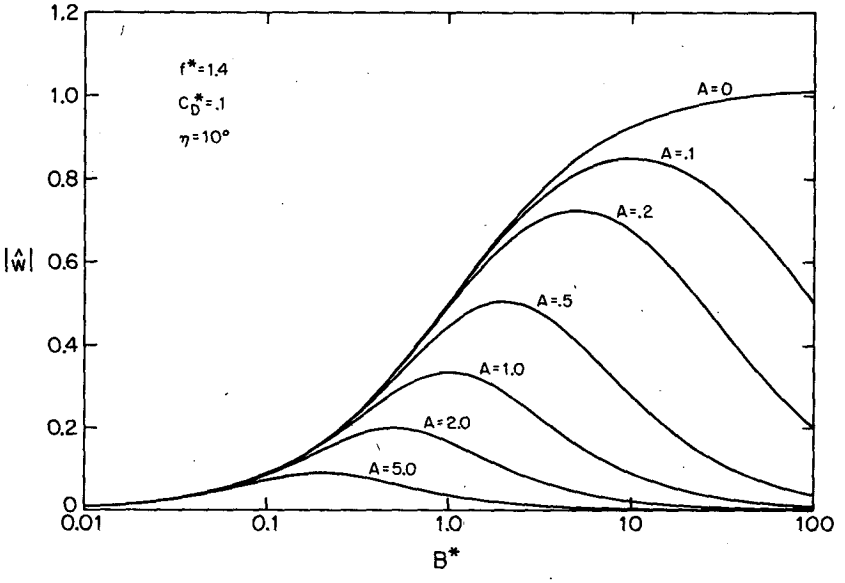


FIG. 7. As in Fig. 4 except for several different values of $A$.

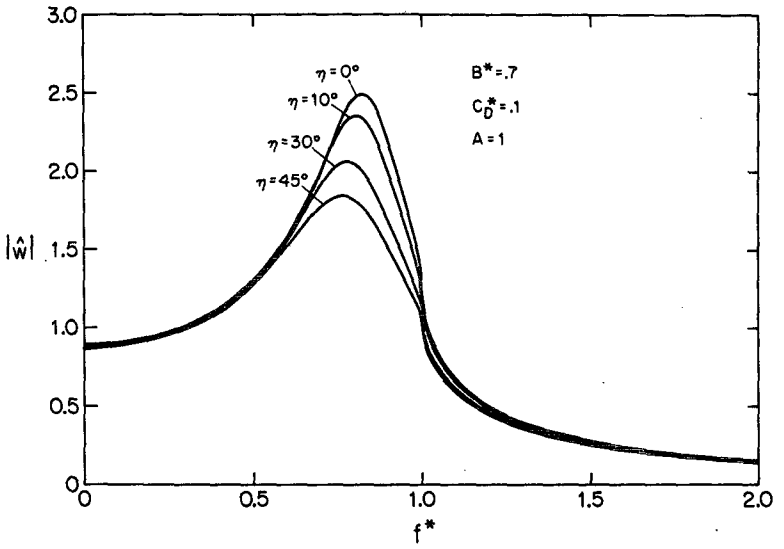


FIG. 8. As in Fig. 2 except for several different values of $\eta$.

When the boundary layer is unstratified (well-mixed), pressure adjustments in the boundary layer vanish as assumed in the classical boundary layer approximation. For this case (Fig. 7, $A = 0$), the vertical motion increases indefinitely with increasing free-flow stratification parameter $B^*$. That is, as the horizontal length scale decreases, suppression of vertical motion by the stratification is now completely offset by increased concentration of convergence, in contrast to the case of nonzero stratification in the boundary layer. This absence of a preferred length scale occurs only poleward of the critical latitude as is made evident by varying $f^*$ (not shown). Equatorward of the critical latitude, a preferred length occurs with $A = 0$ as well as in the case of nonzero stratification in the boundary layer.

Dependence of vertical motion on scaled latitude also indicates a poleward shift of the critical latitude as the relative boundary-layer stratification is decreased.

### *e. Surface stress angle*

Normally the surface stress is directed more toward low pressure compared to the layer-averaged wind. For a given surface drag coefficient, increasing the angle between the surface stress and layer-averaged wind forces the layer-averaged wind to be more oriented in the direction of the geostrophic wind. This reduces the production of cross-isobar flow and vertical motion (Fig. 8). However, this effect is of secondary importance.

### *f. Variation in boundary-layer depth*

As the boundary layer depth increases, $B^*$ increases and $C_D^*$ decreases. Variations in boundary-layer depth (not shown) indicate maximum boundary-layer production of vertical motion at a preferred boundary-layer depth. As the boundary-layer depth increases beyond the preferred value, the boundary-layer depth is no longer thin compared to the oscillating Lineykin layer. Then significant pressure adjustments due to vertical motions occur within the boundary layer. This in turn leads to appreciable reduction of vertical motion at the boundary layer top. As the boundary-layer depth decreases below the preferred depth, the convergence occurs over too thin a layer to generate significant vertical motion.

## 6. Conclusions

Although actual atmospheric boundary layers are much more complicated than the analytical treatment presented here, we have shown that interactions between boundary-layer production of vertical motion and the pressure field will be quite important in certain common atmospheric flow situations. The present study appears to be an improvement on application of Ekman dynamics in that the usage of an eddy viscosity is eliminated and separate boundary layer stratification is included.

When the horizontal length scale of the flow is small and the boundary layer stratification is large, as with nocturnal local flows, pressure adjustments in the boundary layer due to mass convergence will be important. In such cases the usual procedure of specifying the boundary layer pressure field (geostrophic wind) independently of the boundary-layer flow is of limited use. This modification of the boundary-layer pressure field acts to reduce the vertical motion at the top of the boundary layer. The dependence of this reduction of vertical motion on

the boundary-layer stratification can be quantitatively estimated by substituting different values of the corresponding Brunt-Väisälä frequency into (39).

For a given heating gradient, stratification and boundary-layer properties, the maximum vertical motion occurs at a preferred latitude where natural modes of oscillation in the boundary layer have the same frequency as the forcing. These natural modes are influenced not only by the Coriolis parameter and stratification but also by the turbulent transport of heat and momentum. The resulting critical latitude is shifted equatorward from the classical critical latitude associated with Ekman pumping, particularly when stratification within the boundary layer is large.

In the presence of low-level stratification, in and above the boundary layer, we expect the smallest scales of motion to be damped by pressure adjustments. On the other hand, the larger scales are ineffective in concentrating convergence. The intermediate preferred horizontal scale produces the largest vertical motion. This preferred length scale increases with increasing boundary-layer stratification and decreases with distance from the resonant latitude.

The importance of the diurnal-critical latitude in the atmosphere is uncertain although this effect may lead to development of nocturnal thunderstorms as suggested by Paegle and Rasch (1973). They demonstrated that over the Great Plains of the United States, this critical latitude may be shifted poleward due to advections induced by geostrophic vorticity. The present study suggests that this poleward shift and the amplitude of the vertical motion at the top of the boundary layer may be reduced by coupling between the boundary-layer vertical motion and the geostrophic vorticity field, especially with strong boundary-layer stratification and small horizontal length scale of the forcing.

This study also suggests that the strength of local circulations, such as sea and land breezes, may be reduced by stratification within or above the boundary layer. Such circulations may be strongest for a preferred latitude and preferred horizontal length scale.

The above analysis could also be applied to certain aspects of the critical latitude for synoptic scale flow which is often associated with the Intertropical Convergence Zone. Such an application could best be advanced by specifying a time-dependent pressure field as external forcing at the top of the model as in previous models of the critical latitude.

*Acknowledgments*. The comments of the reviewers are greatly appreciated. This work was supported by the National Science Foundation under Grant ATM 79-08308.

## REFERENCES

Arya, S. P. S., and J. C. Wyngaard, 1975: Effect of baroclinity on wind profiles and the geostrophic drag law for the convective planetary boundary layer. *J. Atmos. Sci.*, **32**, 767–778.

Barcilon, V., and J. Pedlosky, 1967: Linear theory of rotating stratified fluid motion. *J. Fluid Mech.*, **29**, 1–16.

Buzyna, C., and G. Veronis, 1971: Spin-up of a stratified fluid: theory and experiment. *J. Fluid Mech.*, **50**, 579–608.

Chang, C. P., 1973: On the depth of the equatorial boundary layer. *J. Atmos. Sci.*, **30**, 436–443.

Clarke, R. H., A. J. Dyer, R. R. Brook, D. G. Reid and A. J. Troup, 1971: The Wangara experiment: Boundary layer data. CSIRO Div. Meteor. Physics, Tech. Pap. No. 19, 336 pp.

Eckart, C., 1960: *Hydrodynamics of Oceans and Atmospheres*. Pergamon Press, 290 pp.

Feynman, R. P., 1964: *The Feynman Lectures on Physics*, Vol. 1. Addison-Wesley, 538 pp.

Greenspan, H. P., and L. N. Howard, 1963: On the time dependent motion of a rotating fluid. *J. Fluid Mech.*, **17**, 385–404.

Hayashi, Y., 1971: Frictional convergence due to large-scale equatorial waves in a finite-depth Ekman layer. *J. Meteor. Soc. Japan*, **49**, 450–456.

Holton, J. R., 1965: The influence of viscous boundary layers on transient motions in a stratified rotating fluid. Part I. *J. Atmos. Sci.*, **22**, 402–411.

——, 1967: The diurnal boundary layer wind oscillation above sloping terrain. *Tellus*, **19**, 199–205.

——, 1975: On the influence of boundary layer friction on mixed Rossby-gravity waves. *Tellus*, **27**, 107–115.

——, J. M. Wallace and J. A. Young, 1971: On boundary layer dynamics and the ITCZ. *J. Atmos. Sci.*, **28**, 275–280.

Kuo, H. L., 1973: Planetary boundary layer flow of a stable atmosphere over the globe. *J. Atmos. Sci.*, **30**, 53–65.

Lineykin, P. S., 1955: On the determination of the thickness of the baroclinic layer in the sea. *Dokl. SSSR Akad. Nauk*, **101**, 461–464.

Mahrt, L., 1974: Time-dependent integrated planetary boundary layer flow. *J. Atmos. Sci.*, **31**, 457–464.

——, and S. U. Park, 1976: The influence of boundary layer pumping on synoptic-scale flow. *J. Atmos. Sci.*, **33**, 1505–1520.

Melgarejo, J. W., and J. W. Deardorff, 1974: Stability functions for the boundary-layer resistance laws based upon observed boundary layer height. *J. Atmos. Sci.*, **31**, 1324–1333.

Merrill, J. T., 1977: Observational and theoretical study of shear instability in air flow near the ground. *J. Atmos. Sci.*, **34**, 911–921.

Paegle, J., and G. Rasch, 1973: Three-dimensional characteristics of diurnally varying boundary-layer flows. *Mon. Wea. Rev.*, **101**, 746–756.

Park, S. U., and L. Mahrt, 1979: Oscillating stratified boundary layers driven by surface temperature variations. *Tellus*, **31**, 254–268.

Shapiro, L. J., 1977: Frictional effects on thermally forced waves. *Tellus*, **29**, 264–271.

Stommel, H., and G. Veronis, 1957: Steady convective motion in a horizontal layer of fluid heated uniformly from above and cooled nonuniformly from below. *Tellus*, **9**, 401–407.

Walin, G., 1969: Some aspects of time-dependent motion of a stratified rotating fluid. *J. Fluid Mech.*, **36**, 289–307.

Walsh, J. E., 1974: Sea breeze theory and applications. *J. Atmos. Sci.*, **31**, 2012–2026.

Yamasaki, M., 1971: Frictional convergence in Rossby waves in low altitudes. *J. Meteor. Soc. Japan*, **49** (Special Issue), 691–698.